ELSEVIER

Physica D 110 (1997) 277–288

PHYSICA D

# Transition to chaos in the conservative four-wave parametric interactions

R. Pakter [a,b], S.R. Lopes [c,*], R.L. Viana [c]

[a] *Instituto de Física, Universidade de São Paulo, Caixa Postal 66318, 05315-970 São Paulo, SP, Brazil*
[b] *Plasma Science and Fusion Center, Massachusetts Institute of Technology, Cambridge, MA 02139, USA*
[c] *Departamento de Física, Universidade Federal do Paraná, Caixa Postal 19081, 81531-990 Curitiba, PR, Brazil*

Received 4 February 1997; received in revised form 14 May 1997; accepted 29 May 1997
Communicated by Y. Kuramoto

**Abstract**

In this work, we analyze the transition from regular to chaotic states in the parametric four-wave interactions. The temporal evolution describing the coupling of two sets of three-waves with quadratic nonlinearity is considered. This system is shown to undergo a chaotic transition via the separatrix chaos scenario, where a soliton-like solution (separatrix) that is found for the integrable (perfect matched) case becomes irregular as a small mismatch is turned on. As the mismatch is increased the separatrix chaotic layer spreads along the phase space, eventually engrossing most part of it. This scenario is typical of low-dimensional Hamiltonian systems.

*PACS:* 05.45.+b; 52.35.Mw; 42.50.Ne
*Keywords:* Hamiltonian chaos; Mode coupling; Plasma; Nonlinear optics

## 1. Introduction

Wave phenomena are of great interest in many branches of physics. In particular, wave–wave interactions are common processes in plasmas and nonlinear optics. Examples of these phenomena can be found in anomalous absorption of laser in laboratory plasmas [1,2], generation of radio emissions in space plasmas [3] and generation of second-harmonic, amplification and frequency-up conversion of optical signals [4,5].

In this paper, we study a particular kind of wave–wave interaction namely, the nonlinear interaction of four waves with two of them participating simultaneously in two resonant triplets. This system was first studied by Sugihara [6] and Karplyuk et al. [7] who have derived some particular solutions for the coupling, considering the case of perfect matching conditions. Extended solutions including negative energy waves were proposed by Walters and Lewak [8] and finally the integrability was proved by the discovery of the fourth intergral of motion [9]. Opposite to the case of a single three-wave triplet, that has received a lot of attention [10,11], the interaction of two sets of three-wave interaction (the resonant four-wave case studied in this paper) is not completely understood.

* Corresponding author.


*PII* S0167-2789(97)00130-9

In a recent paper, Chian et al. [12] have considered the dynamical effects introduced by the presence of frequency mismatch in the wave interaction. They investigated a particular initial condition and proved, by means of Lyapunov exponents, that its trajectory may undergo a transition to chaos as the mismatch is varied. Here we reconsider this problem, fully analyzing both regular (when matching conditions are fulfilled) and chaotic (when the mismatch is introduced) dynamics of a whole set of initial conditions, providing an understanding of the precisely route that leads to the onset of chaos.

In particular, for the regular case it is shown that two distinct groups of periodic solutions are present in the system phase-space. *Dividing* these two phase-space regions we then find a soliton-like solution whose period goes to infinity, i.e., a separatrix. As any finite mismatch is introduced in the system, the non-integrable perturbations drive the separatrix dynamics and its surroundings into chaos, following the typical *sepatrix chaos scenario* [13]. Increasing the mismatch, the separatrix chaotic layer grows, eventually covering most part of the phase-space. The whole chaotization process is accompanied with the aid of conveniently constructed Poincaré plots.

The paper is organized as follows: in Section 2, we introduce the dynamical equations for the resonant four-wave parametric interaction, in Section 3 we discuss some important features of the perfect matched integrable case, in Section 4 the transition to chaotic states when a finite frequency mismatch is introduced is presented and, in Section 5 we conclude the paper.

## 2. Coupled-mode equations

Considering the resonant four-wave parametric interaction involving the coupling of two sets of three-wave with phase-matching conditions of the form

$$\omega_{3,4} = \omega_1 \mp \omega_2 - \delta'_{\mp}, \qquad \mathbf{k}_{3,4} = \mathbf{k}_1 \mp \mathbf{k}_2, \tag{1}$$

where $\delta'_{\mp}$ stand for *small* linear frequency mismatches for each of the two wave triplets. In face of dealing with resonant waves (normal modes) one adopts the modulational notation for the wave fields, $\mathbf{E}_\alpha(\mathbf{x}, t) = \frac{1}{2}\mathcal{E}_\alpha \exp \mathrm{i}(\mathbf{k}_\alpha \cdot \mathbf{x} - \omega_\alpha t) + \text{c.c.}$, where $\mathcal{E}_\alpha(\mathbf{x}, t)$ is a slowly varying complex envelope such that $|\partial_t^2 \mathcal{E}_\alpha| \ll |\omega_\alpha \partial_t \mathcal{E}_\alpha|$ and $|\partial_x^2 \mathcal{E}_\alpha| \ll |k_\alpha \partial_x \mathcal{E}_\alpha|$; $\omega_\alpha(k_\alpha)$ denote the linear dispersion relations of each interacting wave; the subscript $\alpha$ refers to 1–4. Therefore, making use of the fluid equations and Maxwell equations, one is able to write the following set of dynamical equations for the complex envelope of the waves:

$$S_1 \dot{\mathcal{E}}_1 = \sigma \mathcal{E}_2 \mathcal{E}_3 \mathrm{e}^{\mathrm{i}\delta'_- t} - \tau \mathcal{E}_2^* \mathcal{E}_4 \mathrm{e}^{\mathrm{i}\delta'_+ t}, \tag{2}$$

$$S_2 \dot{\mathcal{E}}_2 = -\sigma \mathcal{E}_1 \mathcal{E}_3^* \mathrm{e}^{\mathrm{i}\delta'_- t} - \tau \mathcal{E}_1^* \mathcal{E}_4 \mathrm{e}^{\mathrm{i}\delta'_+ t}, \tag{3}$$

$$S_3 \dot{\mathcal{E}}_3 = -\sigma \mathcal{E}_1 \mathcal{E}_2^* \mathrm{e}^{-\mathrm{i}\delta'_- t}, \tag{4}$$

$$S_4 \dot{\mathcal{E}}_4 = \tau \mathcal{E}_1 \mathcal{E}_2 \mathrm{e}^{-\mathrm{i}\delta'_+ t}, \tag{5}$$

where the dot refers to time derivatives, $\sigma$ and $\tau$ are the time independent interaction kernels determined by the specific physical system one is dealing with $\delta'_- = \omega_1 - \omega_2 - \omega_3$ and $\delta'_+ = \omega_1 + \omega_2 - \omega_4$.

Performing appropriate normalization (see [12] for details) and introducing real variables defined by $\mathcal{E}_\alpha = F_\alpha^{1/2} \mathrm{e}^{\mathrm{i}\phi_\alpha}$, we can re-write the dynamical equations in a form that is more suitable to be analyzed:

$$\dot{F}_1 = 2(F_1 F_2 F_3)^{1/2} \cos\phi_- - 2r(F_1 F_2 F_4)^{1/2} \cos\phi_+, \tag{6}$$

$$\dot{F}_2 = -2(F_1 F_2 F_3)^{1/2} \cos\phi_- - 2r(F_1 F_2 F_4)^{1/2} \cos\phi_+, \tag{7}$$

$$\dot{F}_3 = -2(F_1 F_2 F_3)^{1/2} \cos\phi_-, \tag{8}$$

$$\dot{F}_4 = 2r(F_1F_2F_4)^{1/2}\cos\phi_+, \tag{9}$$

$$\dot{\phi}_- = 1/2(H + \delta_-F_3 + \delta_+F_4)(1/F_2 - 1/F_1) + (F_1F_2/F_3)^{1/2}\sin\phi_- - \delta_-, \tag{10}$$

$$\dot{\phi}_+ = 1/2(H + \delta_-F_3 + \delta_+F_4)(-1/F_2 - 1/F_1) - r(F_1F_2/F_4)^{1/2}\sin\phi_+ - \delta_+, \tag{11}$$

where $H$ is the four-degree of freedom Hamiltonian of the system:

$$H = 2(F_1F_2)^{1/2}(F_3^{1/2}\sin\phi_- - rF_4^{1/2}\sin\phi_+) - \delta_-F_3 - \delta_+F_4, \tag{12}$$

$\phi_- \equiv \phi_1 - \phi_2 - \phi_3$, $\phi_+ \equiv \phi_1 + \phi_2 - \phi_4$ and $\delta_\mp$ are the normalized frequency mismatches. The ratio $r$ measures the relative coupling strengths of the two wave triplets. In the above Hamiltonian formalism $F_\alpha$ and $\phi_\alpha$ are the canonically conjugated coordinate and momentum, respectively.

The system of equations (2)–(5) was first derived by Sugihara [6] in the case of perfect matching, $\delta\mp = 0$, being generalized to include frequency mismatch by Chian et al. [12]. As shown in the latter paper, the inclusion of frequency mismatch leads to the appearance of interesting new features in the non-linear dynamics of the system, specially, the onset of chaos. The aim of this paper is to further analyze these new features, investigating the scenario that leads to the rise of chaos.

## 3. Integrable case and regular solutions

Before fully embarking in the analysis of the dynamics that arise when frequency mismatch is turned on, it is worthwhile spending some time investigating the properties of the regular solutions of the integrable case, $\delta\mp = 0$. This will be done in this section.

In addition to the Hamiltonian given by Eq. (12) the dynamical system of equations (6)–(11) admits other two constants of motion, the so-called Manley–Rowe relations:

$$F_1 + F_3 + F_4 = c_1, \tag{13}$$

$$F_2 - F_3 + F_4 = c_2. \tag{14}$$

Using these relations we are able to remove two pairs of canonical variables from the Hamiltonian, reducing to two the number of degrees of freedom of the system. This will be treated in more detail later on.

Moreover, a fourth independent constant of motion was found by Romeiras [9], thus proving the general integrability of the system. The use of this constant in order to analyze the properties of the solutions of the system is not a trivial task. However, if we concentrate ourselves on a special set of initial conditions, namely those with $H = 0$, much more tractable solutions may be found. In fact, these initial conditions are not only of didactical interest, but also of practical importance since they encompass those situations typically found in decay instability where one or more of the four waves initially vanishes.

Following Refs. [7,8], using $H = 0$ and working with Eqs. (2)–(5) we find three others constants of motion, $c_3$, $c_4$ and $c_5$, to be given by

$$F_3^{1/2}\sin\phi_- = c_3, \tag{15}$$

$$F_4^{1/2}\sin\phi_+ = c_4, \tag{16}$$

$$|F_3^{1/2}\cos\phi_- + (1/r)F_4^{1/2}\cos\phi_+| = c_5. \tag{17}$$

In the last equation it is necessary to take the absolute value since the expression on the left-hand side presents a constant modulus but keeps varying its signal due to discontinuous changes in the angle variables $\phi_-$ and $\phi_+$.

Now defining the variable

$$X = sF_3^{1/2}\cos\phi_-, \tag{18}$$

where $s = \pm 1$ stands for the signal of the left-hand side expression in Eq. (17) without the modulus and is conveniently used in order to avoid discontinuities in the dynamics of $X$, one can write a closed equation in the form

$$\left(\frac{\mathrm{d}X}{\mathrm{d}t}\right)^2 + V(X) = 0 \tag{19}$$

with $V(X)$ as an effective potential that drives the motion of the variable given by

$$V(X) = -[c_1 - c_3^2 - X^2 - c_4^2 - r^2(X - c_5)^2][c_2 + c_3^2 + X^2 - c_4^2 - r^2(X - c_5)^2]. \tag{20}$$

Although Eq. (19) can be solved in terms of elliptic functions, and from $X(t)$ and the constants of motion $c_i$ we could find the time evolution of any $F_\alpha$, here we will not be interested in the explicit solutions but instead in investigating some features of the solution that appears as we vary the initial conditions. This can be done by seeking for the roots of $V(X)$ and noting that since $(\mathrm{d}X/\mathrm{d}t)^2$ must be always positive, the motion of $X$ is constrained to the *potential well* between two of the roots of $V(X)$.

For future purposes that will become clear in the Section 4, we will focus on sets of initial conditions that have not only the same Hamiltonian value ($H = 0$), but also the same values for the constants $c_1$ and $c_2$. A very simple set that fulfills these requirements is the following:

$$\begin{aligned} &F_1(t=0) = c_1 - \eta, \qquad F_2(t=0) = c_2 - \eta, \\ &F_3(t=0) = 0, \quad F_4(t=0) = \eta, \quad \phi_-(t=0) = \pi, \quad \phi_+(t=0) = 0 \end{aligned} \tag{21}$$

with $\eta$ as the parameter labeling the different initial conditions and whose values vary from 0 to lesser between $c_1$ and $c_2$, since $F_{1,2}$ must be positive. As we are concerned with decay processes, we typically have $c_2 \ll c_1$ and $0 \leq \eta \leq c_2$. The set of initial conditions presented in Eqs. (21) is such that $c_3 = c_4 = 0$, $c_5 = \sqrt{\eta}/r$ and $X(t=0) = 0$.

To start with the analysis of the different types of motion that may occur as we vary $\eta$, we first write the roots of the effective potential equation (20) for the set of initial condition we are interested in:

$$X_{1,2} = \frac{r\eta^{1/2} \mp \sqrt{(r^2+1)c_1 - \eta}}{r^2+1}, \tag{22}$$

$$X_{3,4} = \frac{r\eta^{1/2} \mp \sqrt{(r^2-1)c_2 + \eta}}{r^2-1} \tag{23}$$

with $X_{1,3}$ corresponding to the minus sign and $X_{2,4}$ to the plus sign.

Let us first consider the simplest care $r = 1$. A quick inspection either on the expression for $V(X)$ or on Eqs. (22) and (23) reveals that for this value of the relative coupling strengths parameter only three roots exist; $X_4$ is no longer present, and $X_3$ assumes the value $X_3 = (\eta - c_2)/2\eta^{1/2}$. The effective potential and the respective time evolution for the wave amplitudes $F_\alpha$ are shown in Figs. 1 and 2 for different values of the initial condition parameter $\eta$ with $c_1 = 10$ and $c_2 = 1$, typical of a decay process. For $\eta = 0$, curve (a) of Figs. 1 and 2(a), which actually is the initial condition analyzed in [12], we find that $X_3$ diverges to minus infinity and $V(X)$ is negative between $X_1$ and $X_2$, roots that are symmetric with respect to $X = 0$, i.e. $X$ oscillates between $\pm X_1 = \mp(c_1/2)^{1/2}$. The implication of the symmetry in the motion of $X$ is that $F_1$ has the same value for all its minima as it is seen in Fig. 2(a). For this special case, $F_2$ presents no dynamics, acting just as a *catalyst* in the interaction [8] and $F_3$ and $F_4$ undergo the same

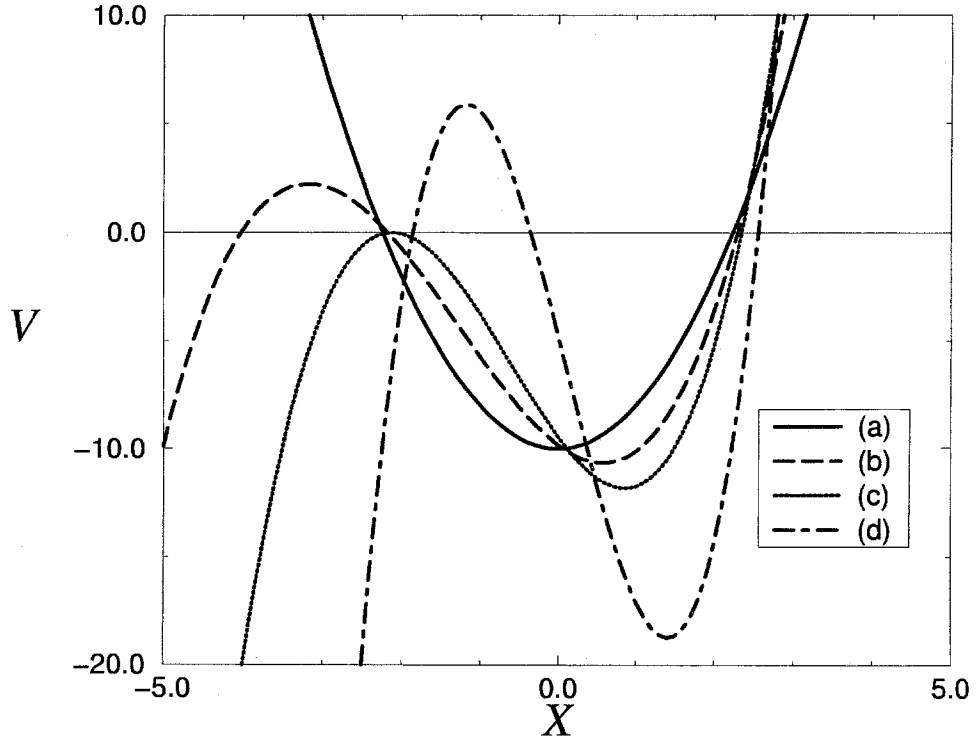


Fig. 1. Effective Potential $V(X)$ for the set of initial conditions, Eq. (21), with $r = 1$, $c_1 = 10$, $c_2 = 1$, and (a) $\eta = 0$, (b) $\eta = 0.015$, (c) $\eta = \eta_2^* = 10 - \sqrt{99}$ and (d) $\eta = 0.5$.

evolution. Increasing the value of $\eta$, as shown in Figs. 1 (curve (b)) and 2(b) for $\eta = 0.015$, the root $X_3$ starts to migrate in the direction of $X = 0$, with $X_1$ and $X_2$ *nearly* keeping their symmetry since $\eta \ll c_1$. As a consequence, $F_1$ and $F_2$ *nearly* present the same values for all their maxima and minima. For a critical value of $\eta$, namely $\eta_2^*$ (see Eq. (26)), the potential exhibits a double root at $X = X_1 = X_3$ as found in Fig. 1 (curve (c)). Hence, the period of motion of $X$ and, consequently, of the $F_\alpha$ tend to infinity giving rise to a soliton-like solution, i.e. a separatrix of the system. This solution is presented in Fig. 2(c). Above $\eta = \eta_2^*$ the roots become such that $X_3 > X_1$ and the *potential well* is found for $X$ between $X_3$ and $X_2$ (curve (d) of Fig. 1). Now the motion of $X$ is asymmetric and the $F_\alpha$ present very distinct values in their successive maxima and minima presented in Fig. 2(d).

Physically, the emergence of the two different types of solutions discussed above, that may be roughly divided into the nearly symmetric ones and the asymmetric ones, is understood as follows. For $\eta = 0$, one has that the hole of waves four and three are the same, both of them grow pumped by the decay of wave one or decay to waves two and one synchronized in time. As $\eta$ grows to a finite value wave four is not synchronized with wave three anymore, so that a second small deep (because of the decay of wave one into wave four) in the series of wave one can be seen.

By virtue of the effective potential equation (20) one is able to investigate the dynamics of $X$ for other values of the parameter $r$. The main results of such investigation are presented in Table 1. There appears the critcal values $r^*$, $\eta_1^*$ and $\eta_2^*$ defined as

$$r^* = \left(\frac{c_1 - c_2}{c_1 + c_2}\right)^{1/2}, \tag{24}$$

$$\eta_1^* = (1 - r^2)c_2, \tag{25}$$

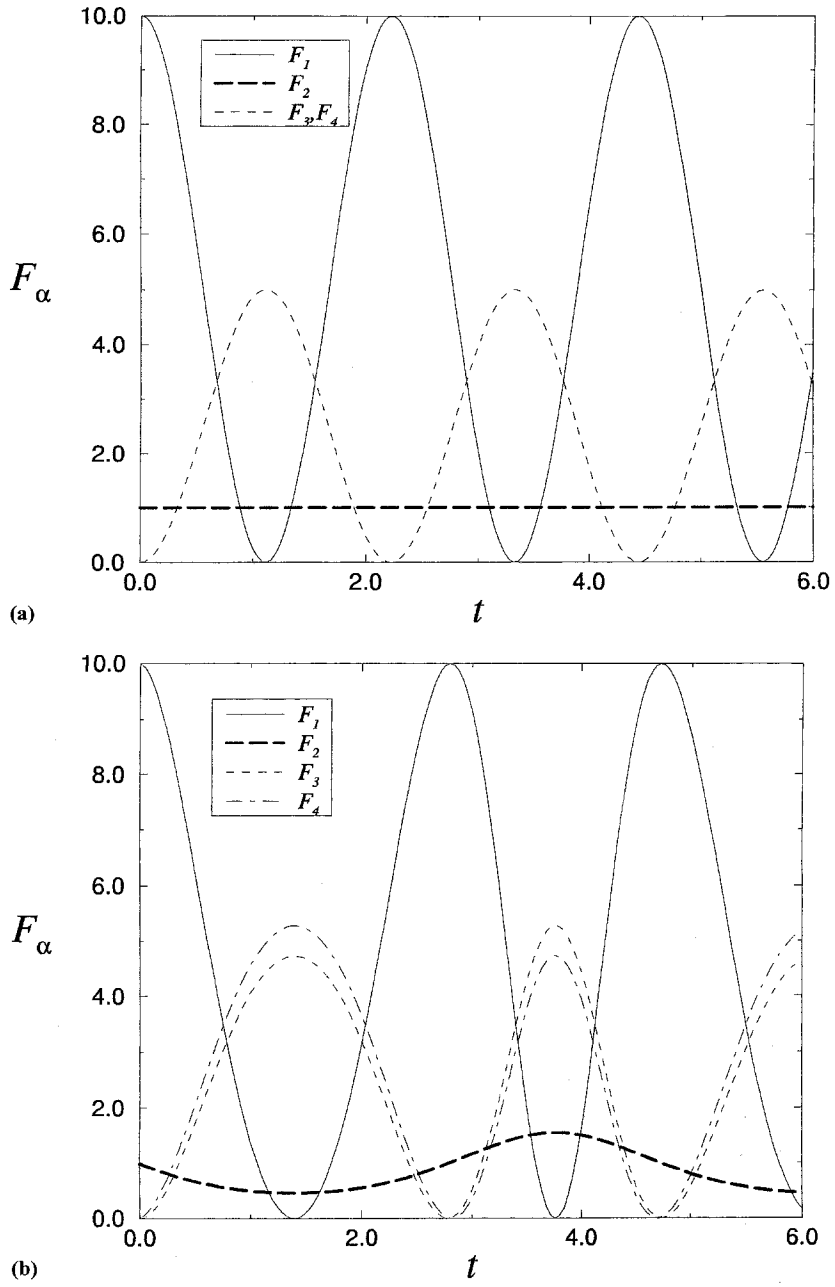


Fig. 2. Time evolution of the wave amplitudes $F_\alpha$ for the same initial conditions used in Fig. 1.

$$\eta_2^* = \left(\frac{1+r^2}{2}\right) c_1 + \left(\frac{1-r^2}{2}\right) c_2 - r(c_1^2 - c_2^2)^{1/2}. \tag{26}$$

The contents of Table 1 reveal that, similar to the $r = 1$ case discussed above in detail, irrespective to the value of $r$ it is typically found two types of solutions for the system as the initial conditions are varied. Moreover, in

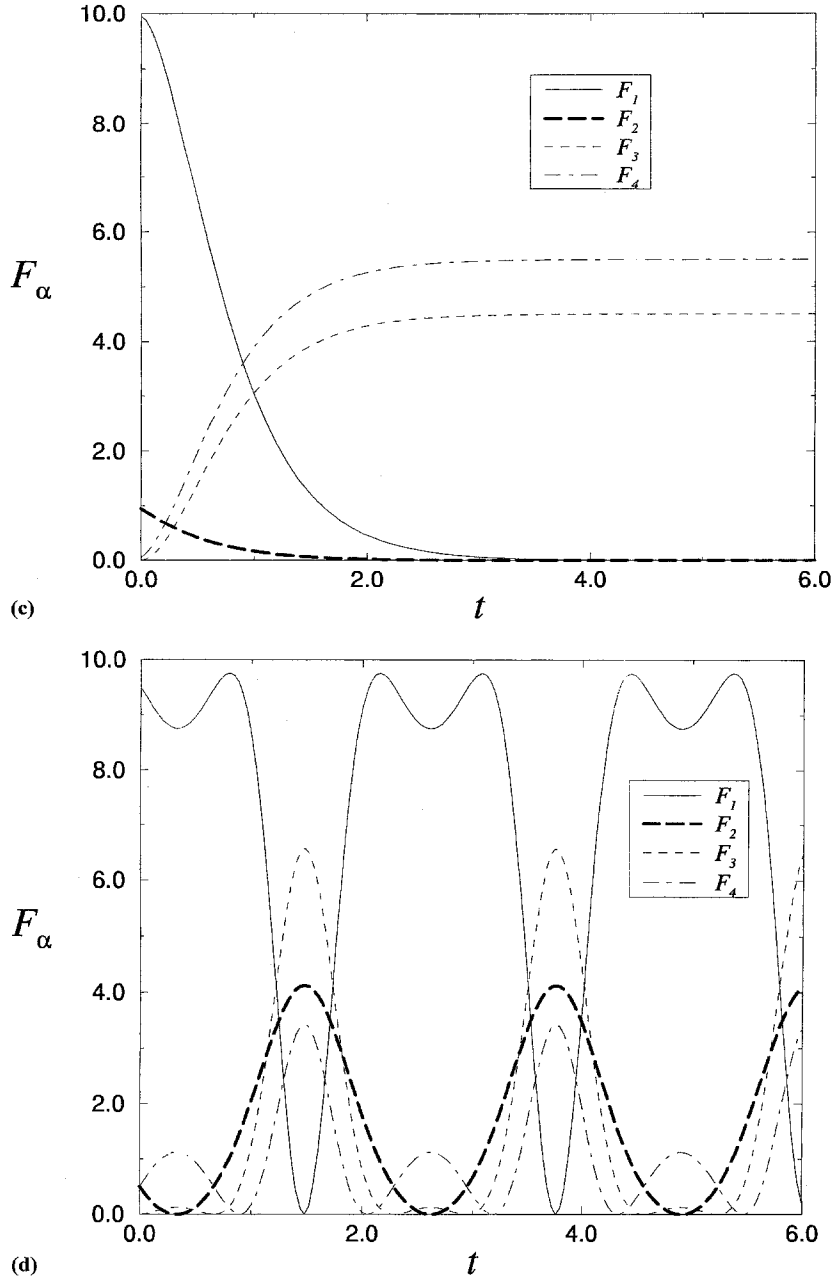


Fig. 2. Continued

the transition between these different types of solutions the period of the orbits goes to infinity, therefore inducing the appearance of a soliton-like solution connected to a separatrix of the system. As will be shown in the next section, the existence of the separatrix orbit plays a crucial role in the nonlinear dynamics of the coupled-mode interaction.

Table 1
Analysis of the dynamics of $X \equiv sF_3 \cos\phi_-$ by means of the effective potential $V(X)$, Eq. (20), for different values of $r$ and $\eta$

| $r$ | $\eta$ | Roots | Remarks |
|---|---|---|---|
| $r < r^*$ | $\eta < \eta_1^*$ | $\{X_1 < X_2\}$ | $X_3, X_4$ complex |
| | $\eta = \eta_1^*$ | $X_1 < \{X_3 = X_4 < X_2\}$ | Separatrix |
| | $\eta_1^* < \eta < \eta_2^*$ | $X_1 < X_4 < \{X_3 < X_2\}$ | |
| | $\eta = \eta_2^*$ | $X_1 = X_4 < \{X_3 < X_2\}$ | |
| | $\eta > \eta_2^*$ | $X_4 < X_1 < \{X_3 < X_2\}$ | |
| $r = r^*$ | $\eta < \eta_1^*$ | $\{X_1 < X_2\}$ | $X_3, X_4$ complex |
| | $\eta = \eta_1^*$ | $\{X_1 = X_3 = X_4 < X_2\}$ | Separatrix (triple root) |
| | $\eta > \eta_1^*$ | $X_4 < X_1 < \{X_3 < X_2\}$ | |
| $r^* < r < 1$ | $\eta < \eta_1^*$ | $\{X_1 < X_2\}$ | $X_3, X_4$ complex |
| | $\eta = \eta_1^*$ | $X_4 = X_3 < \{X_1 < X_2\}$ | |
| | $\eta_1^* < \eta < \eta_2^*$ | $X_4 < X_3 < \{X_1 < X_2\}$ | |
| | $\eta = \eta_2^*$ | $X_4 < \{X_3 = X_1 < X_2\}$ | Separatrix |
| | $\eta > \eta_2^*$ | $X_4 < X_1 < \{X_3 < X_2\}$ | |
| $r = 1$ | $\eta < \eta_2^*$ | $X_3 < \{X_1 < X_2\}$ | |
| | $\eta = \eta_2^*$ | $\{X_3 = X_1 < X_2\}$ | Separatrix |
| | $\eta > \eta_2^*$ | $X_1 < \{X_3 < X_2\}$ | |
| $1 < r < 1/r^*$ | $\eta < \eta_2^*$ | $X_3 < \{X_1 < X_2\} < X_4$ | |
| | $\eta = \eta_2^*$ | $\{X_3 = X_1 < X_2\} < X_4$ | Separatrix |
| | $\eta > \eta_2^*$ | $X_1 < \{X_3 < X_2\} < X_4$ | |
| $r = 1/r^*$ | $\eta = 0$ | $\{X_3 = X_1 < X_2 = X_4\}$ | Separatrix (two double roots) |
| | $\eta > 0$ | $X_1 < \{X_3 < X_2\} < X_4$ | |
| $r > 1/r^*$ | $\eta < \eta_2^*$ | $X_1 < \{X_3 < X_4\} < X_2$ | |
| | $\eta = \eta_2^*$ | $X_1 < \{X_3 < X_4 = X_2\}$ | Separatrix |
| | $\eta > \eta_2^*$ | $X_1 < \{X_3 < X_2\} < X_4$ | |

The motion is constrained to the roots between curly brackets. Critical values $r^*$, $\eta_1^*$ and $\eta_2^*$ are defined in Eqs. (24)–(26).

## 4. Mismatched case: Transition to chaos

Let us now proceed to the analysis of the case where there is a linear frequency mismatch. Recalling some discussions of the previous section, when $\delta_\mp = 0$ four independent (in the sense that they are in involution) constants of motion can be found to assure the integrability of the four-degree of freedom system described by the Hamiltonian equation (12). These constants are: the one found by Romeiras [9], the Manley–Rowe relations (13) and (14) and, of course, the Hamiltonian itself. For the special case $H = 0$, the former one may be replaced by the constants defined in Eqs. (15)–(17) and the system becomes *super-integrable* (note, however, that $c_3$ and $c_4$ are dependents), presenting more constants in involution than degrees of freedom [14].

As a finite frequency mismatch is turned on, the scenario presented above is changed. Although the constancy of the Hamiltonian and the Manley–Rowe relations remain valid, neither the constant found by Romeiras [9], nor any of the $c_{3,4,5}$ defined in Eqs. (15)–(17) persist. Hence, the system turns to have more degrees of freedom than constants of motion and chaos is likely to be found. Actually, the presence of chaotic motion was confirmed by Chian et al. [12] who found positive Lyapunov exponents in the dynamics of the mismatched system. Our aim here is to further analyze the transition from the regular motion previously discussed, enlightening the processes that drive dynamics into chaos.

Our investigations will be based on the analysis of Poincaré plots constructed from the numerical integration of the motion equations of the system in their complex form and we will set $\delta_+ = 0$ and let $\delta_-$ as a free parameter. In order to build up convenient plots it is necessary to take into consideration some aspects to be treated now. First of all, note that all the initial conditions must be chosen in such a way that they lead to the same values for all the constants of motion $H$, $c_1$ and $c_2$. Not surprisingly this is exactly the case for the initial conditions afore considered, given by Eqs. (21). Another important subject matter concerns the choice of the coordinates to be plotted each time the Poincaré section is pierced. At this point, we realize that until now we have not explicitly used the constants of motion we have at hands to effectively reduce the number of degrees of freedom of the system. This can be properly done by introducing a generating function of the form

$$\mathcal{F}_2(\{F_\alpha, \phi'_\alpha\}) = F_1\phi'_1 + F_2\phi'_2 + (F_1 - F_2 + 2F_3)\phi'_3 + (F_1 + F_2 + 2F_4)\phi'_4, \tag{27}$$

that leads to the following canonical transformation equations:

$$\begin{aligned} F'_1 &= F_1, & \phi'_1 &= (\phi_+ + \phi_-)/2, \\ F'_2 &= F_2, & \phi'_2 &= (\phi_+ - \phi_-)/2, \\ F'_3 &= F_1 - F_2 + 2F_3 = c_1 - c_2, & \phi'_3 &= \phi_3/2, \\ F'_4 &= F_1 + F_2 + 2F_4 = c_1 + c_2, & \phi'_4 &= \phi_4/2, \end{aligned}$$

where the primes indicate transformed variables. Note that $F_1$ and $F_2$ have no transformation and so we will drop their primes from now on. The Hamiltonian assumes the form

$$\begin{aligned} H = (F_1F_2/2)^{1/2}&[(F'_3 - F_1 + F_2)^{1/2}\sin(\phi'_1 - \phi'_2) \\ &-r(F'_4 - F_1 - F_2)^{1/2}\sin(\phi'_1 + \phi'_2)] - \delta_-(F'_3 - F_1 + F_2)/2. \end{aligned} \tag{28}$$

As a matter of fact, $\phi'_3$ and $\phi'_4$ are cyclic and $F'_3$ and $F'_4$ are now constants. Finally, we choose to plot the pair $\{\phi'_2, F_2\}$ each time $F_1$ has a minimum.

In general, it would be interesting to start by exploring Poincaré plots made for the integrable case $\delta_- = 0$, so we would probably get some notion of the system we are dealing with. However, taking into account that for $\delta_- = 0$ the initial conditions we are considering ($H = 0$) lead to a *super-integrable* system, in attempting to construct the plots we would find that each initial condition pierces the Poincaré section in a finite number of points that form no structures (curves), thus giving no useful information.

Hence, let us begin our analysis for a small but finite value of the mismatch parameter. In Fig. 3(a) the Poincaré plot is presented for $\delta_- = 0.01$. Constants $c_1$ and $c_2$ are the same as in the previous figures and we will focus on the case $r = 1$, remarking however, that following the discussions of the Section 3, similar conclusions are expected for other values of $r$. Note that instead of plotting the phase $\phi'_2$ which is $\pi$-periodic, we are using $\phi_+ - \phi_- = 2\phi'_2$ that is properly $2\pi$-periodic. One can easily see the presence of two distinct resonant islands separated by a thin chaotic layer. Comparing the values of the initial condition parameter $\eta$ for the different structures that are present, we were led to the conclusion that the *lower* resonant island in Fig. 3(a) refers to the symmetric solutions found for $\eta < \eta_2^*$ in the integrable case, and the *upper* one, to the asymmetric solutions found for $\eta > \eta_2^*$. In fact, these two islands present different periods as it is shown in Fig. 3(b), where we plot a linear-log version of Fig. 3(a). There we realize that the former is actually period one, while the latter is period two, piercing the Poincaré Plot once for $F_2 \ll 1$ and then for $F_2 \sim 1$–10. Moreover, as it could be expected [13], the chaotic layer in the intermediate region between the different island chains is found for initial conditions near the separatrix value $\eta = \eta_2^*$. As the value of the mismatch parameter is increased up to $\delta = 0.1$, Fig. 3(c), one can readily see the enlargement of the chaotic region and the occurrence of phase-locked states that appear as secondary resonant islands surrounding the fixed points of the map. The appearance of such structures is another signature of the non-integrability of the system. Further increasing $\delta$,

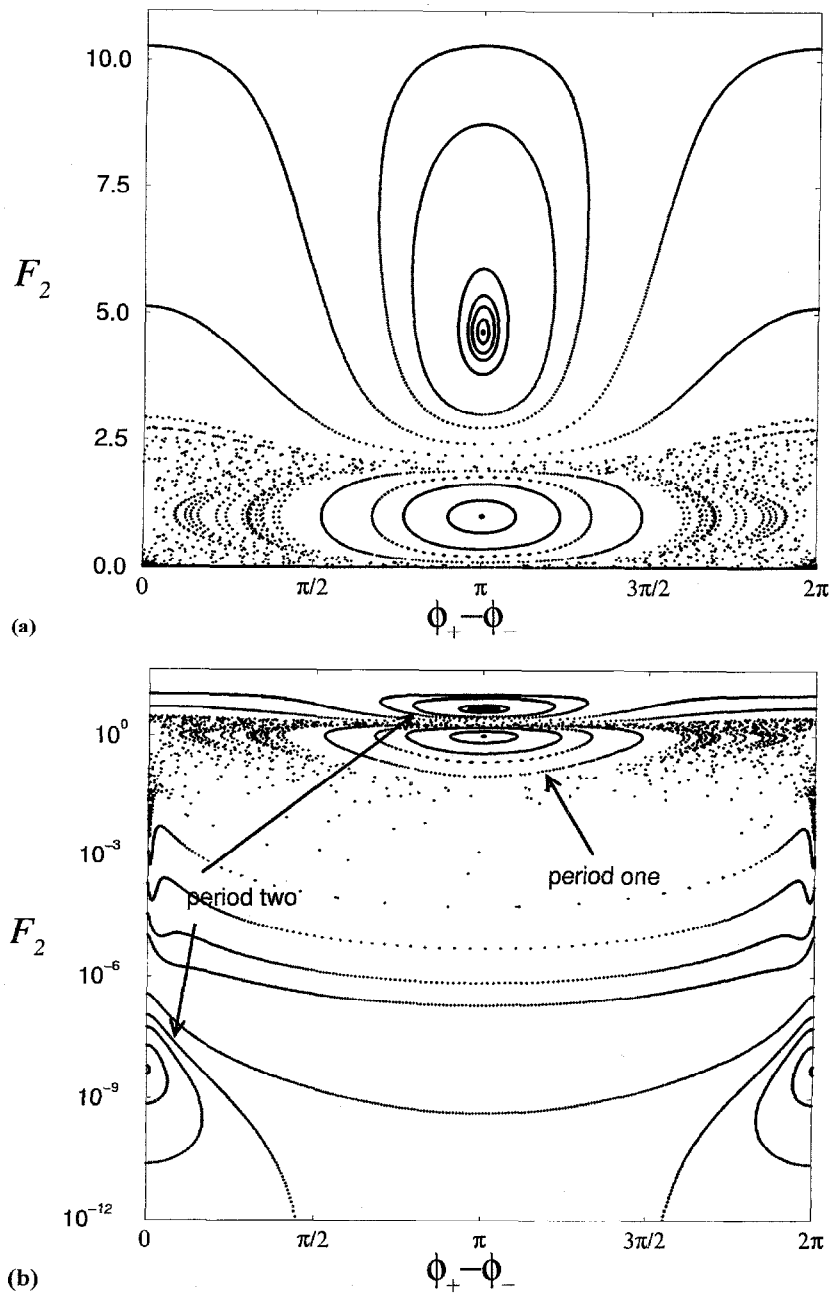


Fig. 3. Poincaré plot of $F_2$ vs. $(\phi_+ - \phi_-)$ for the mismatched case with $r = 1$, $c_1 = 10$ and $c_2 = 1$. In (a) and (b) $\delta = 0.01$ (a) has a linear scale, while (b) has a linear-log scale in order to show in more detail the $F_2 \ll 1$ portion of the phase-space), in (c) $\delta = 0.1$, and in (d) $\delta = 0.5$.

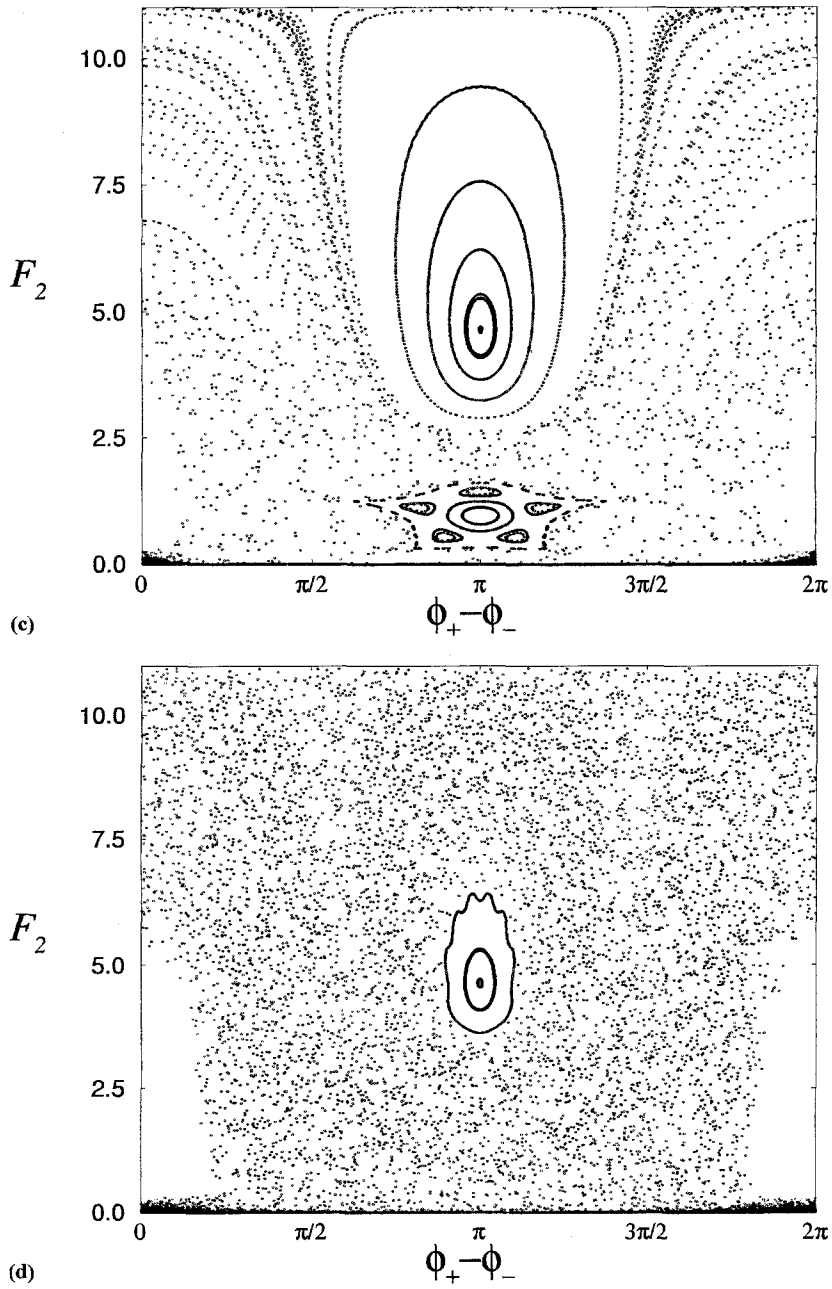


Fig. 3. Continued

Fig. 3(d), we find an almost completely destroyed Poincaré Plot with the chaotic region engrossing the major part of the phase-space. It becomes clear from these last figures that there is a growing (with $\delta$) portion of the phase space, namely around $\phi_+ - \phi_- \approx 0$ $(2\pi)$ and $F_2 \approx 2.0$, where no trajectory pierces the Poincaré Plot. It is worthwhile mentioning that the existence of this portion is not related to any KAM curves that may be present there, but to

the occurrence of a forbidden region where it is impossible to satisfy the mapping condition $\dot{F}_1 = 0$ for the given parameter values [15].

## 5. Conclusion

In this paper we have analyzed the transition to chaos in the resonant four-wave interaction involving the coupling of two sets of three-waves. In the absence of frequency mismatch this system is integrable presenting typically two distinct types of periodic solutions, and a soliton-like solution as the initial conditions are varied. By means of conveniently constructed Poincaré plots we have shown that in presence of frequency mismatch the afore mentioned two types of solutions give rise to two island chains of different periodicity, with a chaotic layer (relative to the soliton-like solution) between them. Thus, characterizing the separatrix chaos scenario. As the value of the frequency mismatch parameter was increased the spreading of the chaotic layer was verified over the major part of the phase-space, leading to the chaotization of basically all initial conditions.

## Acknowledgements

The authors are grateful to F.B. Rizzato, I.L. Caldas, L.P.L. Oliveira, G. Corso and A.C.-L. Chian for discussions. This work was supported by $CNP_q$, FINEP and CAPES, Brazil. Numerical computing was partially performed on the CRAY Y-MP2E at the Universidabe Federal do Rio Grande do Sul Supercomputing Center.

## References

[1] W.L. Kruer, The Physics of Laser Plasma Interactions (Addison-Wesley, Redwood City, 1988).
[2] A.C.-L. Chian and F.B. Rizzato, Coupling of electromagnetic filamentation instability and electrostatic Langmuir parametric instabilities in laser-plasma interactions, J. Plasma Phys. 51 (1994) 61–73.
[3] A.C.-L. Chian, S.R. Lopes and M.V. Alves, Generation of auroral whistler-mode radiation via nonlinear coupling of Langmuir waves and Alfvén waves, Astron. Astrophys. 290 (1994) L13–L16.
[4] Y.R. Shen, The Principle of Nonlinear Optics (Wiley, New York, 1984).
[5] A. Yariv, Quantum Electronics (Wiley, New York, 1989).
[6] R. Sugihara, Interaction between an electromagnetic wave, plasma waves, and an ion acoustic wave, Phys. Fluids 11 (1968) 178–184.
[7] K.S. Karplyuk, V.N. Oraevskii and V.P. Pavlenko, Dynamics of the nonlinear interaction of magnetohydrodynamic waves, J. Plasma Phys. 15 (1973) 113–124.
[8] D. Walters and G.J. Lewak, Dynamics of four coupled plasma waves to second order, J. Plasma Phys. 18 (1977) 525–536.
[9] F.J. Romeiras, Integrability of double three-wave interaction, Phys. Lett. A 93 (1983) 227–229.
[10] S.R. Lopes and A.C.-L. Chian, Controlling chaos in nonlinear three-wave coupling, Phys. Rev. E 54 (1996) 170.
[11] J.M. Wersinger, J.M. Finn and E. Ott, Bifurcations and strange behavior in instability saturation by nonlinear mode coupling, Phys. Rev. Lett. 44 (1980) 453–456.
[12] A.C.-L. Chian, S.R. Lopes and J.R. Abalde, Hamiltonian chaos in two coupled three-wave parametric interactions with quadratic nonlinearity, Physica D 99 (1996) 269–275.
[13] A.J. Lichtenberg and M.A. Lieberman, Regular and Stochastic Motion (Springer, New York, 1983).
[14] J. Hietarinta, Direct methods for the search of the second invariant, Phys. Rep. 147 (1987) 87.
[15] R. Pakter, I.L. Caldas, F. Couto, T. Caetano and F.B. Rizzato, Chaotic dynamics induced by space-charge waves in cyclotron resonance accelerators, Phys. Rev. E 54 (1996) 4202.